13C.3 EXAMINING TROPICAL CYCLONE STRUCTURE VARIABILITY USING H*WIND ANALYSES

Robert A. Stenger and Russell L. Elsberry *
Naval Postgraduate School, Monterey, California

1. INTRODUCTION

Hurricanes are among the most costly natural disasters in the United States as a result of strong winds (Pielke and Landsea 1998) and flooding (Elsberry 2002). In recent years, the landfall of large hurricanes in densely populated areas along the Gulf Coast of the United States has increased the awareness that tropical cyclone structure plays an important role in the destructive potential of a storm (Powell and Reinhold 2007). The tropical cyclone structure change can be quite large over relatively short periods of time. Without a complete understanding of these structure variations, accurate wind and surge forecasting for tropical cyclone damage potential will remain elusive.

In the Unites States, the emergency management community requires warnings of when sustained (one-minute average) surface winds exceeding gale-force (≥ 34 kt) winds will arrive at a location in advance of a tropical cyclone. That is, the objective is to give the public sufficient time to complete all disaster preparedness activities prior to when gale-force winds (usually accompanied by heavy precipitation) arrive, so that these activities (including evacuation or moving to a secure shelter) are completed safely.

While an accurate understanding of structure change for landfalling cyclones is a concern to populated coastal regions, they are equally important to commercial shipping vessels, and the airplanes and warships of the United States Air Force and Navy and those of its allies. When a threat of damaging 50-kt winds exists from a tropical cyclone within 48 hours, the Air Force will evacuate airborne assets and personnel to inland locations. Airborne assets that are not flight-ready and are not repairable within a reasonable amount of time must be placed inside a hangar and tied down. Total evacuation of a military base is very costly, but the direct impact of damaging tropical cyclone winds can be devastating. Unfortunately, our inability to forecast tropical cyclone track, intensity, and structure with great accuracy leads decision makers to error on the side of safety and results in unnecessary expenditure of funds for false alarms.

As for the Navy, surface vessels that are under way must remain outside the radius of gale-force winds. Since there is little certainty in our ability to forecast tropical cyclone structure, ships must remain well beyond the perimeter of danger. This leads to increased fuel costs and lost time to missions within the assigned area of operations. In addition, a naval surface fleet that is in port must be sortied when a tropical cyclone is a threat to the port. Once again, uncertainty can lead to the unnecessary expenditure of tax dollars (as much as 15 million dollars) when the forecast results in a false alarm.

Whereas much of the recent tropical cyclone structure research has focused on the intensity, the focus in this paper is on the outer wind structure of tropical cyclones. The importance of the outer wind structure for tropical cyclone motion will be reviewed in section 2, with an illustration of the empirical wind profiles that have been previously used to describe the wind structure. More complex outer wind profiles associated with secondary eyewalls and annular tropical cyclones will be described in section 3. The implications of empirical wind profiles as in section 2 and idealized numerical models for wind structure change are described in section 4. A simple wind structure change model tied to intensification and decay phases is tested in section 5 and found to not explain many observed changes. The variability of tropical cyclone outer wind structure is presented in section 6 for both the standard Saffir-Simpson storm categories and for the stages of storm development discussed in section 5.2. Finally, some conclusions are made in section 7.

2. TRACK DEPENDENCY ON OUTER WIND STRUCTURE

Fiorino and Elsberry (1989) emphasized the importance of the outer wind structure for the beta-effect propagation (BEP) component of tropical cyclone motion. Using a non-divergent barotropic model, they demonstrated that the BEP was unchanged if the inner (within 300 km in their vortex simulation) wind profiles had intensities varying from 20 m s^{-1} to 50 m s^{-1}. However, corresponding changes in the outer (beyond 300 km) wind profiles changed the BEP significantly. That is, larger storms (stronger winds in outer region) have a larger poleward and westward BEP speed.

Carr and Elsberry (1997) derived a simple wind structure relationship based on angular momentum concepts

$$v(r) = \frac{M}{r^x} - \frac{1}{2} f_o r \qquad (1)$$

where v is the tangential wind as a function of radius r, f_o is the Coriolis parameter at the latitude of the storm center, and the exponent x is given as 0.4. The constant $M = 0.5 f_o R_o^{1+x}$ is specified at a radius R_o where the cyclonic tangential wind goes to zero, which might then be considered as another "size" measure of

* *Corresponding author address:* Russell L. Elsberry, GSEAS, Department of Meteorology, Naval Postgraduate School, 589 Dyer Rd., Room 254, Monterey, CA 93943-5114; e-mail: Elsberry@nps.edu

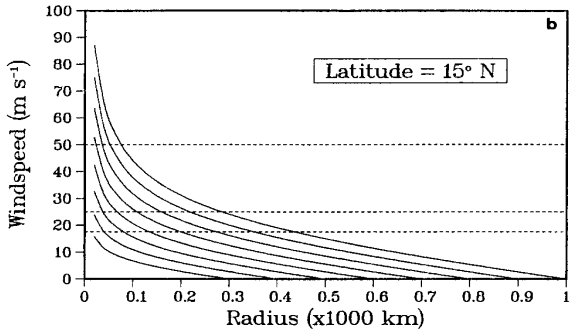

Fig. 1. Tangential wind profiles for Carr and Elsberry (1997) with X = 0.4 for various radial extents R_o at the latitude of 15° latitude. Threshold wind speeds of 17, 25, and 50 m s^{-1} are highlighted by horizontal dashed lines.

the tropical cyclone. Examples of the resulting tangential wind profiles with radius for different values of R_o in a storm at 15° latitude are given in Fig. 1. At large radii where the winds are small, and thus frictional effects are small, the wind profile is determined by conservation of *earth* angular momentum that the air parcel has at the radius R_o where the *relative* angular momentum is equal to zero. Thus, the outer tangential wind increases almost linearly with radius toward the center since the last term in Eq. (1) depends on the first power of radius. In the inner-core region, which may then be defined as the region where frictional influences are large and angular momentum is not conserved, the wind speed increases more rapidly toward the center as the first term in Eq. (1) is dominant. Following Fiorino and Elsberry (1989), Carr and Elsberry (1997) demonstrate that outer wind profiles beginning at large values of R_o have much larger BEP values.

Several numerical weather prediction (NWP) centers (e.g., Japan Meteorological Agency, U.S. Fleet Numerical Meteorology and Oceanography Center) use empirical relationships to specify the outer wind structure in tropical cyclones because inadequate observations are available. Thus, two NWP models with different specifications of the outer wind structures in the tropical cyclone would predict different tracks even if everything else (observations, data assimilation, model characteristics) were identical. So improved observations, understanding, and prediction of outer wind structure will also lead to improved track forecasts, which will lead to better wind warnings for the public.

3. MORE COMPLEX OUTER WIND PROFILES

3.1 Secondary Eyewalls

Willoughby et al. (1982) described secondary eyewalls in which a concentric ring of convection develops at an outer radii, and these convective regions have an associated wind maximum that is not included in simple profiles as in Fig. 1. Rather, a profile as in Fig. 1 outward from the radius of maximum wind would adjust to another relative wind maximum at the radius of the secondary eyewall with a decreasing wind profile farther outward from that maximum. Because the secondary eyewalls in the cases described by Willoughby et al. (1982) tended to contract inward, progressively larger wind speeds evolved at smaller radii as in the modified Rankine vortex ($v\, r^{x}$ = constant). Meanwhile, the maximum wind speed (i.e., the intensity) in association with the inner eyewall decreased such that it became smaller than the wind speed associated with the secondary eyewall. This evolution has been termed an *eyewall replacement cycle*, although it is not clear that the inner eyewall cloud band always disappears. A more general characterization by Elsberry et al. (2007) of the life cycle intensity changes used below is a decay and re-intensification cycle (Stage IIa).

Based on microwave imagery during 1997-2005, Hawkins et al. (2006) observed that 80% (70%, 50%, 40%) of the tropical cyclones in the western North Pacific (Atlantic, eastern North Pacific, Southern Hemisphere) with maximum winds exceeding 120 kt had one or more secondary eyewall formations.

One may expect the outer wind speeds would increase, and the radius of 34-kt winds would increase, if an external physical mechanism that led to the secondary eyewall as in Fig. 1 with the same exponent x = 0.4. Alternately, an internal mechanism might create the secondary eyewall wind maximum and simultaneously "spin-up" the wind speeds at outer radii along a profile as in Fig. 1.

A high-resolution numerical simulation by Terwey and Montgomery (2008) led to an intense vortex (87 m s^{-1}) at a relatively small radius (30 km) that was then followed by a secondary eyewall formation. As shown in Fig. 2, the inner wind maximum decreased until around Hour 180 the outer wind maximum at 80 km was stronger (65 m s^{-1}), which would be designated as an eyewall

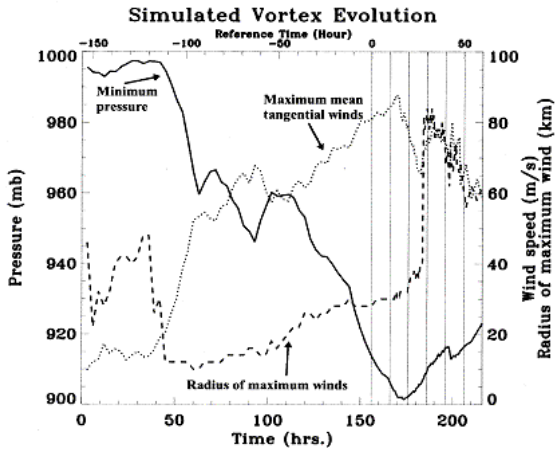

Fig. 2. Modeled storm evolution through the simulation time for the control experiment. The solid line is the minimum pressure at 150 m above the surface. The dashed line is the radius of maximum mean tangential winds at 150 m above the surface. The dotted line is the maximum azimuthally averaged tangential winds through the domain.

replacement cycle. Terwey and Montgomery do not display the outer wind profiles before and after the secondary eyewall formation and eyewall replacement cycle. To demonstrate the potential magnitude of the outer wind structure changes, a modified Rankine vortex with an exponent x = 0.5 was assumed. Given the two wind maxima and corresponding radii in Fig. 2 (and given above), the 50-kt wind radius would increase from 360 km to 541 km, and the 34-kt wind radius would increase from 783 km to 1171 km. These (likely excessive) outer wind radii increases from before to after a secondary eyewall formation and eyewall replacement cycle suggest large outer wind structure modifications during such events. Another possible implication of such an event occurring as the tropical cyclone was approaching the coast would be a sudden decrease in the disaster preparation time needed before gale-force winds would be reaching the coast.

3.2 Annular Tropical Cyclones

Under favorable environmental conditions, a tropical cyclone can form a stable, persistent axisymmetric wind structure coined as "annular" by Knaff et al. (2003). The formation of this special structure has been shown to be systematic through asymmetric mixing between the eye and eyewall of a storm involving one or two mesovortices. Annular tropical cyclones present a significant challenge to forecasters since their behavior does not follow the climatological norms of storm evolution or intensity. Intensity tendencies of annular systems indicate that these storms maintain their intensity longer than the average tropical cyclone with a mean intensity of greater than 100 kt.

Knaff et al. (2003) examined the characteristics of six annular hurricanes that occurred in the Atlantic and eastern North Pacific basins from 1995-1999. The following characteristics were found to separate annular hurricanes from the general population of hurricanes: (i) a nearly circular eye size with a larger than average radii; (ii) a symmetric annulus of deep convection with small asymmetries in cloud-top brightness temperatures; and (iii) a general lack of deep convective features, such as spiral rainbands, beyond the annulus of deep convection surrounding the eye. Furthermore, Knaff et al. (2003) found environmental conditions to be favorable for annular hurricane development when: (i) there was relatively weak wind shear that was easterly in the deep layer (850-200 hPa) and east-southeasterly in the shallow layer (850-500 hPa); (ii) easterly flow and colder than average temperatures at 200 hPa; and (iii) nearly constant sea-surface temperatures (SST) in the range of 25.4-28.5°C.

Because Knaff et al. (2003) found that the formation of annular hurricanes appeared after an asymmetric mixing of the eye and eyewall components via mesovortices, it is assumed here that prior to becoming an annular hurricane, the storm was quite intense. Indeed, the discriminant analysis technique proposed by Knaff et al. (2008) for objectively identifying an annular hurricane in the Atlantic and eastern North Pacific performs best if all hurricanes with intensities ≤ 84 kt are first eliminated. For the six (eight) Atlantic (eastern North Pacific) annular hurricanes that they identified during 1995-2006, the minimum intensity was 100 kt (90 kt). Annular typhoons also exist, but it is unknown if the same SST, minimum intensity, and other thresholds apply.

Given that annular tropical cyclones form a secondary eyewall during an intense stage, it will be assumed that a similarity exists with the secondary eyewall formations discussed in subsection 3a above. For the 14 annular hurricanes during 1995-2006, the mean radius of the lowest azimuthally-averaged cloud-top temperatures (i.e., eyewall radius) was 81 km, with a minimum of 62 km, and a maximum of 128 km. With a minimum intensity of 90 kt at such large radii, the outer wind speeds would likely be larger than for an average hurricane. The differences are assumed to be: (i) annular tropical cyclones form from an *internal* mechanism following an eyewall mixing event in which the intense inner wind maximum is diminished; and (ii) the outer (secondary) eyewall is stable to radial deflections (rather than contracting) due to special environmental conditions listed above.

The relevance to outer wind structure changes is similar to that in subsection 3.1, i.e., forming an intense outer wind maximum in an annular tropical cyclone is likely to increase the 34-kt wind radius.

4. IDEALIZED TROPICAL CYCLONE STRUCTURE CHANGES

The implication from an empirical wind profile such as in Fig. 1 is that the outer- and inner-core wind structure vary together. That is, physical processes that increase/decrease the intensity would have a corresponding increase/decrease in the entire wind structure. In this simple model, the outer winds would increase during the intensification stage and would decrease during the weakening stage of the tropical cyclone life cycle.

In the idealized axisymmetric models of the intensification stage, a similar scenario occurs with outer wind speed increases following the spin-up of the inner core. In the Emanuel (1995a, b) model, the temperature profile is assumed to be moist-neutral at each radius, so that the entire vertical profile is known given the temperature and moisture near the surface, and from hydrostatic equation the surface pressure is known. Given an initial cyclonic vortex (typical maximum wind speed of 10 m s^{-1} at a radius of 150 km), the frictional forces lead to an inflow, and the air parcels acquire heat and moisture from the warm ocean as they approach the center. The purpose of the model is to estimate the intensity from the thermal and moisture conditions that are predicted to exist at the bottom of the eyewall cloud. However, the assumption of a moist-neutral atmosphere tied to the near-surface temperature and moisture radial profile provides the radial profile of the pressure field at all levels as well, and thus the outer wind structure.

As in the case of the empirical wind profile in Fig. 1, the outer wind increases in the axisymmetric model will be directly correlated with the intensity increases, which in the idealized model are determined by the sea-surface temperature and upper-tropospheric

temperatures at which the outflow is assumed to occur. Except for the imposed temperature and moisture profiles at large radius, the outer conditions are tied to the inner core prediction – the values of wind or momentum at the outer boundary are assumed to not be important.

5. ACTUAL STRUCTURE CHANGES

5.1 Conceptual Model of Outer Wind Structure Changes

If the tropical wind structure changes are driven by the inner-core processes, the implication from empirical wind profile reasoning or the idealized, axisymmetric models would be that the outer winds would increase during the intensification stage and decrease during the decaying stage. Whereas the forecaster rules of thumb are compatible with the idea of increasing outer winds during the intensification stage, the general expectation (e.g., Merrill 1984) is that the tropical cyclone size expands (i.e., outer winds at a radius would be increasing) during the decay or extratropical transition stage. Especially in the case of extratropical transition in which the tropical cyclone is moving into the midlatitude westerlies, the apparent expansion may be due to the circulation being superposed on an environment with stronger winds.

Kimball and Mulekar (2004) produced a 15-year climatology of the six size parameters from the extended best track dataset of North Atlantic tropical cyclones. Kimball and Mulekar calculated the means, medians, and standard deviations of the radii of the eye, maximum winds, hurricane-force winds, damaging-force winds (defined at 25.7 m s^{-1}), gale-force winds, and the outer-most closed isobar. The advantage of the Atlantic dataset is that aircraft reconnaissance observations are available in most of the tropical cyclones west of 55°W, which allows the calculation of these wind radii that are not directly observed in other basins that do not have aircraft reconnaissance. A possible disadvantage is the practice to include ex-tropical cyclones in the Atlantic dataset that may bias the statistics compared to other basins in which the tropical cyclones are only considered to exist in much lower latitudes.

Kimball and Mulekar (2004) construct a climatological evolution of the Saffir-Simpson categories based on the median values of the various radii (Fig. 3). Note that the outer winds also increase as the intensity increases from Tropical Storm (TS) stage to Category 1 hurricanes (H1) in Fig. 3a. However, the R_{34} value did not increase from Category 1 to Category 2 (not shown), and then did increase from Category 2 to Category 3. As shown in Fig. 3b, the median R_{34} value for the Category 4 hurricanes actually decrease relative to the Category 3 value, which is different from the simple model of an increase in outer wind structure during intensification. The caution is that this climatological model of hurricane evolution is based on median values in each category in the sample rather than the evolution of individual cyclones.

Knaff et al. (2007) have developed a climatological and persistence technique for predicting the wind radii

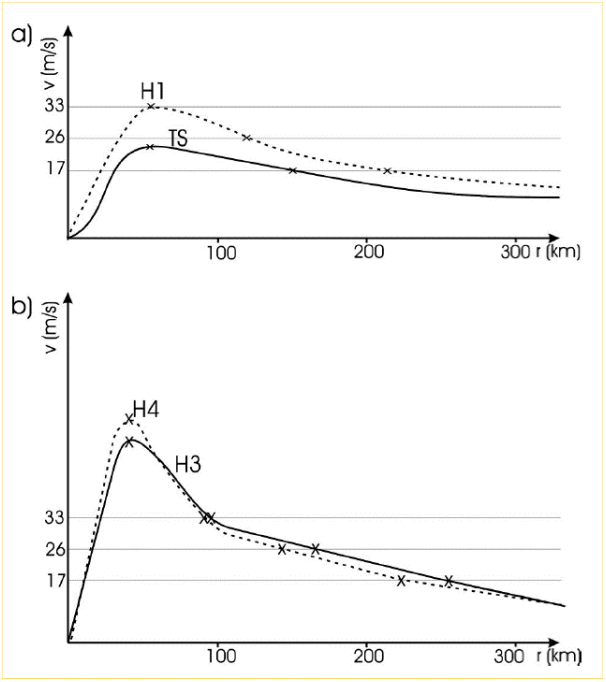

Fig. 3. Median tangential wind profiles from Kimball and Mulekar (2004) for Atlantic (a) tropical storms (TS) versus Saffir-Simpson Category 1 (H1) hurricanes and (b) Category 3 (H3) and Category 4 (H4) hurricanes.

evolution each 12 h to 120 h. The key step in their technique is the fitting of the wind profile to the operational estimates of the 34, 50, and 64 kt radii. Their climatological wind profile has a symmetrical component with a modified Rankine profile that varies with latitude, storm translation speed, and maximum wind with statistical relationships derived from a 1998-2004 dataset in the Atlantic and 2001-2004 in the North Pacific basins. In particular, the increase in tangential winds toward the center in the modified Rankine profile is more (less) rapid for all larger intensity tropical cyclones and below (above) 25°N latitude. In practice, the departures of operational estimates from this climatological wind profile are calculated and the deviations from climatology are assumed to decay over the 120-h forecast period based on a statistical persistence relationship. Because the persistence decay function decreases rapidly from 0.45 – 0.68 at 12 h to a value of 0.10 by 30 h – 60 h (Fig.1; Knaff et al., 2007), the "forecasts" after these times are essentially a reversion to the climatological profile. Since the climatological profile is a modified Rankine profile tied to the maximum wind and a radius of maximum wind speeds for tropical cyclones at latitudes less than 25°N. For latitudes north of 25°N, the contribution of the increasing latitudinal effect, especially with a decreasing maximum wind speed, will then broaden the vortex (smaller value of x-exponent in the modified Rankine vortex).

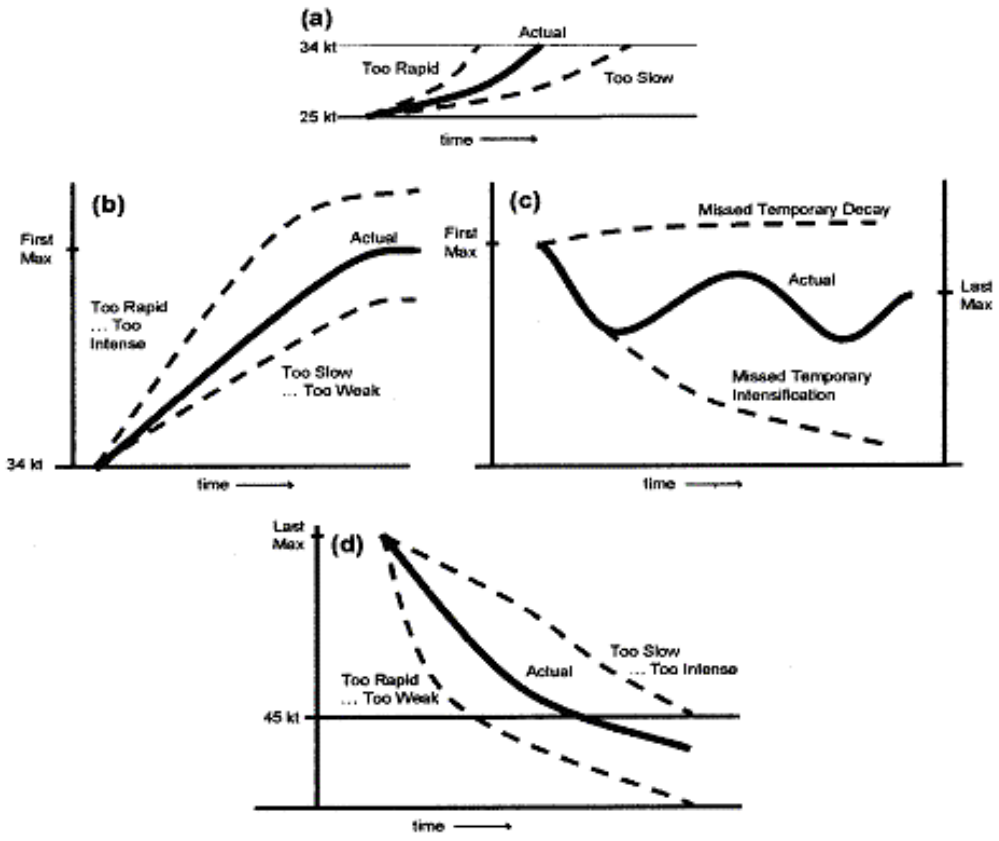

Fig. 4. Definitions by Elsberry et al. (2007) of intensity change phases during the life cycle of a tropical cyclone (a) phase I, formation; (b) phase II, intensification; (c) phase IIa, decay and re-intensification cycle; and (d) phase III, decay. See text for specific definitions.

5.2 Data Set of Surface Wind Analyses

Elsberry and Stenger (2008) tested these simple conceptual ideas of outer wind structure changes through application of the tropical cyclone life cycle intensity change definitions of Elsberry et al. (2007) displayed in Fig. 4. The Elsberry et al. (2007) formation Stage I is limited to V_{max} less than 34 kt. Storm intensification from 34 kt to the first intensity peak (or end of this stage) is defined as Stage II. After the first intensity peak, if the storm intensity decays by at least 10 kt and then re-intensifies by at least 10 kt, it is defined as a decay and re-intensification cycle that is labeled as Stage IIa. If the re-intensification criterion of Stage IIa is not met, the storm is decaying and classified as Stage III. In addition, Stage II is subdivided into rapid or non-rapid intensification, and Stage IIa is subdivided into a decay followed by either a rapid or a non-rapid intensification. Rapid intensification is defined here as an increase equal to or greater than 15 kt in 12 h. A 12-h interval was selected to better capture rapid intensification events during storm intensity cycles and exclude intensity fluctuations that occur over shorter periods of time.

The unique data set Elsberry and Stenger (2008) used to study outer wind structure change was from the National Oceanic and Atmospheric Administration (NOAA)-Atlantic Oceanographic and Meteorological Laboratory (AOML) Hurricane Wind Analysis System (H*Wind; Powell et al. 1996, 1998). The H*Wind grid is centered on the storm and has a horizontal grid spacing of approximately 6 km in a domain of 920 km by 920 km. The H*Wind analyses incorporate all available surface observations, such as ships, buoys, coastal platforms, surface aviation reports, and reconnaissance aircraft data adjusted to the surface (NOAA 2007). Observations that are fit to the analysis framework include data transmitted from NOAA P-3 research aircraft equipped with the Stepped Frequency Microwave Radiometer (SFMR) flown by the Hurricane Research Division (HRD), and the United States Air Force Reserve (AFRES) C-130 reconnaissance aircraft flight-level winds. Additional sources of data include remotely sensed winds from the polar-orbiting satellite platforms of Special Sensor Microwave/Imager (SSM/I) and European Remote Sensing (ERS), the microwave imagers of QuikScat and Tropical Rainfall Measuring Mission (TRMM), and Geostationary Operational Environmental Satellites (GOES) drift winds from the geostationary satellites. All data are processed to conform to the common height of 10 m and an averaging period of 1-minute maximum sustained wind speed.

Fig. 5. Time series of outer wind structure changes in terms of radius of 50-kt winds (R_{50}) and of 34-kt winds (R_{34}) in each Cartesian quadrant for Hurricane Ivan (2004) comparing values for H*Wind analyses that include only aircraft flight-level reductions or SRMR estimates.

The H*Wind analyses are not without limitations. It is possible that V_{max} in a given tropical cyclone might not be sampled during the typical radial reconnaissance along four azimuthal flight legs during the 4-6 h period required for an analysis (Powell and Reinhold 2007). Uncertainty of the analyzed V_{max} depends on data coverage and the quality of the data from the individual platforms contributing to the final analysis. Uncertainty is estimated at 10 percent when the peak wind is measured within the eyewall by the SFMR-equipped aircraft, or if measured outside the eyewall where *in situ* observations are more plentiful. It is estimated that uncertainty is approximately 20 percent when the peak wind within the eyewall is measured using a simple reduction of flight-level wind data to the surface. H*Wind analyses are generally not available east of 50°W longitude in the Atlantic basin due to the limits imposed by available basing locations and flight duration of airborne assets given the fuel load.

Elsberry and Stenger (2008) analyzed 35 tropical cyclones that occurred in the Atlantic and three tropical cyclones that occurred in the eastern North Pacific basins from 2003 through 2005. During this period, 571 H*Wind analyses were produced. However, the raw fields for six analysis times were unavailable, and one field was eliminated due to suspect wind values. The remaining 564 H*Wind analyses contain dropsonde data in 508 analyses, aircraft flight-level reduced data in 470 analyses (hereafter referred to as “aircraft FLR data”), and 135 analyses with SFMR data. Dropsonde data were generally absent from eastern North Pacific tropical cyclones and for weak storms. Dropsonde, aircraft FLR, and SFMR data were simultaneously available in 55 of the H*Wind analyses. However, most analyses contain a combination of dropsondes and aircraft FLR data, or dropsondes and SFMR data.

Those H*Wind analyses that include the SFMR observations are considered to have the most reliable representation of the surface wind fields because of the continuous profiles along the radial flight paths of the aircraft. Due to the limited number of analyses with SFMR data, it was necessary to include surface wind analyses that were primarily based on the reduction of aircraft flight-level winds (usually flown at 700 mb). A comparison of the time evolution of R_{34} and R_{50} for Hurricane Ivan (2004) using mutually exclusive analyses that contain SFMR data versus aircraft flight-level reduction is given in Fig. 5 for different quadrants of the storm. The differences between these wind radii derived from H*Wind analyses based primarily on these two data sources are within the range of variability depicted by the aircraft FLR data. Other storm cases have a similar agreement as in Fig. 5.

5.3 Observed Outer Wind Structure Changes During Life Cycle

Histograms of 12-h axisymmetric outer wind structure changes in terms of R_{34} values are shown in Figs. 6-8. These calculations of axisymmetric wind structure are computed along 24 equally-spaced radial legs at

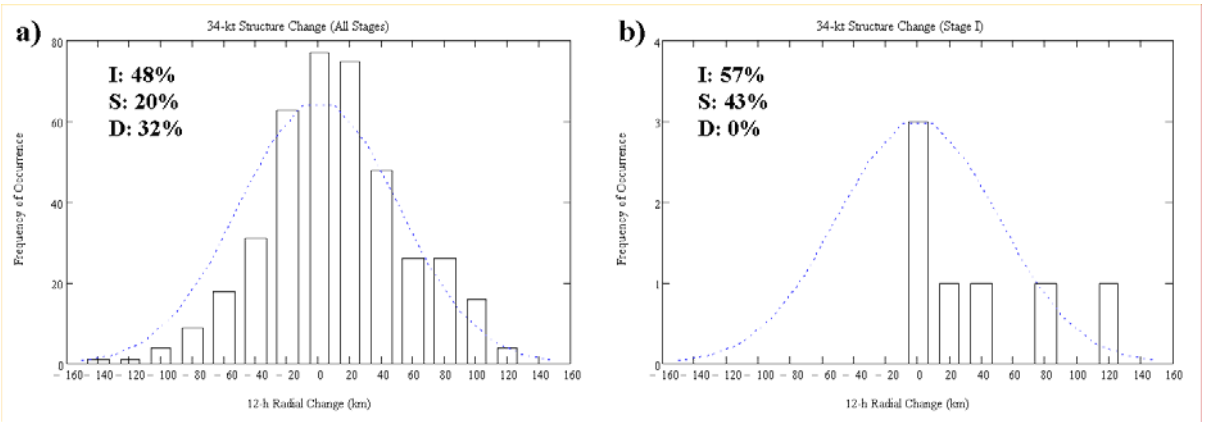

Fig. 6. Histograms of 12-h axisymmetric outer wind structure changes in terms of R_{34} values for (a) All H*Wind analyses and (b) Stage I of the life cycle as in Fig. 3. The percentage of storms exhibiting and increase (I), steady (S), or decrease (D) in structure size are listed in the upper-left corner of each histogram. The dashed line is a normal Gaussian distribution.

consecutive rings spaced every 6 km from the center of the tropical cyclone. It is important to note that all quadrants in which land intersects the 34-kt wind radii are eliminated from the calculations, but no fewer than two quadrants or 13 radial legs are used in the calculation at any analysis time. After eliminating all cases that involve landfall, or where insufficient analyses are available to compute the 12-h structure change, 400 cases remained to evaluate R_{34} structure variability during the 2003-2005 Atlantic tropical cyclone seasons.

Without consideration of the life cycle stage, the histogram for the all-sample of 12-h changes in R_{34} approximates a Gaussian distribution (Fig. 6, dashed line). A bias toward positive 12-h R_{34} changes is evident in this sample that includes all stages. Outer wind structure changes in terms of 12-h R_{34} values between ± 10 km were deemed as steady state, and the clustering of values in this range appears to be justified by the distribution, if not a little conservative. Note that the changes in the axisymmetrical radial structure in the entire sample can be quite large over a 12-h period, with values as large as ±135 km. For a hurricane approaching a coastline at 5 m s^{-1}, an undetected 12-h expansion of the gale-force wind radius by 135 km would decrease the preparation time by about 8 hours.

Only a very small sample of H*Wind analyses are available for the Formation Stage I as defined in Fig. 4. Thus, the histogram of 12-h R_{34} changes for Stage I in Fig. 6b should be viewed as tentative. This limited sample of R_{34} change values does seem to indicate a general tendency toward an expansion in size during the formation stage. It is noteworthy that one expansion of 120 km in 12 h was documented. Given the limitations of this sample, it seems unlikely that a larger sample will make the distribution more Gaussian. The tendency for positive increases in R_{34} in the formation stage is consistent with the expectation of the empirical profiles as in Fig. 1 and the axisymmetric models discussed in section 4.

The histograms for 12-h R_{34} changes during rapid (Fig. 7a) and non-rapid (Fig. 7b) intensification during Stage II suggest a tendency for more increases (54% and 56%, respectively) than decreases (32% and 28%) in outer wind speeds. The non-rapid intensification following a decay in Stage IIa has similar percentages (Fig. 7d) of positive (54%) and negative (26%) 12-h R_{34} changes. For the rapid intensifications following a decay in Stage IIa (Fig. 7c), the percentages of positive (44%) and negative (33%) 12-h R_{34} changes are more nearly balanced, and with a large percentage of steady-state (± 10 km) conditions (23%). The relatively large number of decreases in the R_{34} values for the intensification Stages II and IIa does not agree with the expectations from the empirical wind distribution in Fig. 1 or the axisymmetric models that would suggest an increase in outer winds (R_{34}) during intensification. Thus, further study is required to understand the physical processes that lead to a decrease in R_{34} during intensification.

The histogram for 12-h R_{34} changes during the Decay Stage III (Fig. 8b) indicates a tendency for more negative (49%) than positive (26%) values, with a considerable fraction of steady-state conditions (± 10 km). Approach to land may account for some shift toward negative R_{34} changes in the distribution during the Decay Stage III, whereas storms such as Hurricane Ophelia during 2005 shrunk in size while at higher latitudes with little or no intensity change, no significant land interaction, and under weak vertical wind shear conditions. By contrast, the 12-h R_{34} changes during the decay stage of the Stage IIa decay and re-intensification cycle (Fig. 8a) has proportionally more increases (51%) than decreases (37%), and has a distribution that approaches Gaussian centered on + 20 km increase in R_{34} over 12 h. Recall that a decrease in R_{34} values during the decay stage might be expected from the empirical wind profile in Fig. 1, and from subsequent solutions of the axisymmetric model to fit a

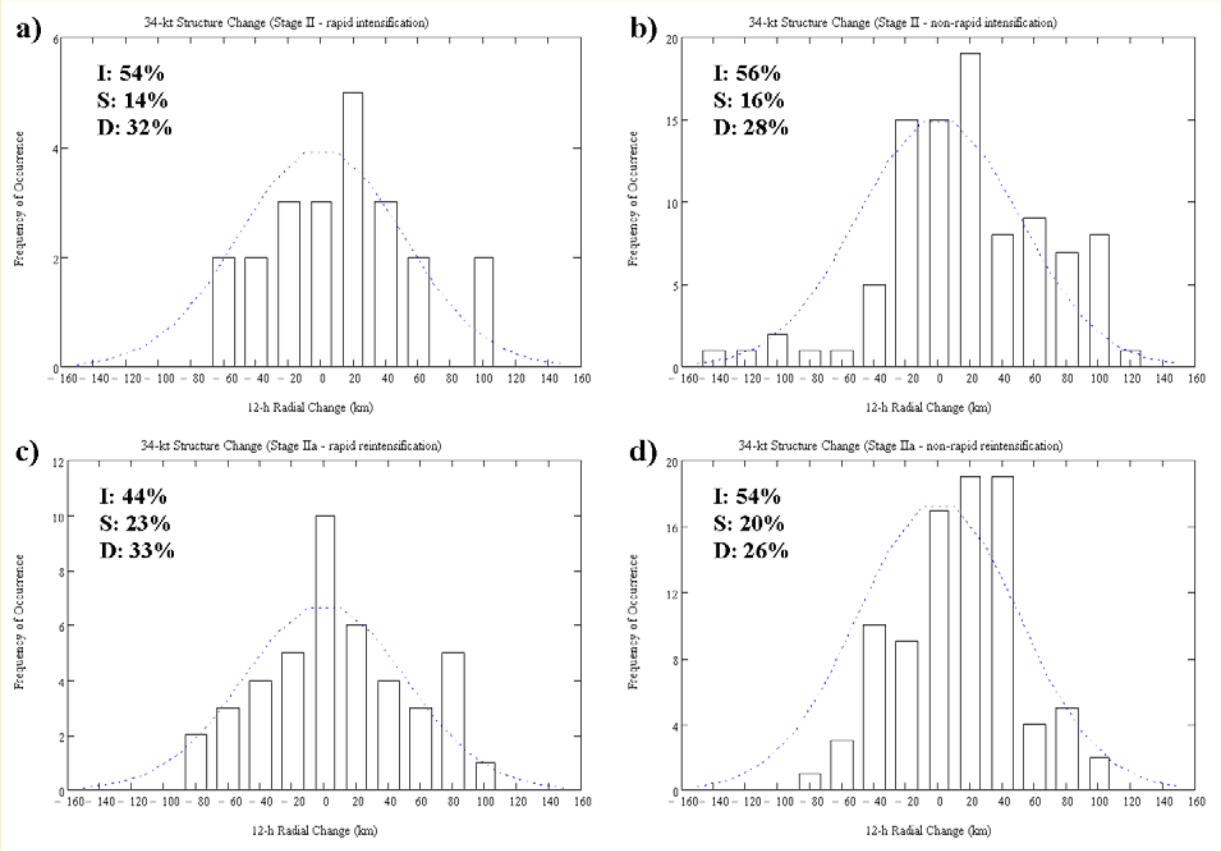

Fig. 7. Histograms of 12-h axisymmetric outer wind structure changes in terms of R_{34} values as in Fig. 6, except for (a) Stage II – rapid intensification, (b) Stage II – non-rapid intensification, (c) Stage IIa - rapid intensification, and (d) Stage IIa – non-rapid intensification.

decreasing intensity. By contrast, the forecaster rule-of-thumb is to expect an increase in the size during the decay of tropical cyclones (Merrill 1988). Again, further study is required to understand the physical processes that lead to both decreases and increases in the outer winds when the tropical cyclone intensity is decreasing either in the Stage IIa decay or the final decay in Stage III.

The histograms for R_{50} and R_{64} changes (not shown) have similar distributions for the different life cycle

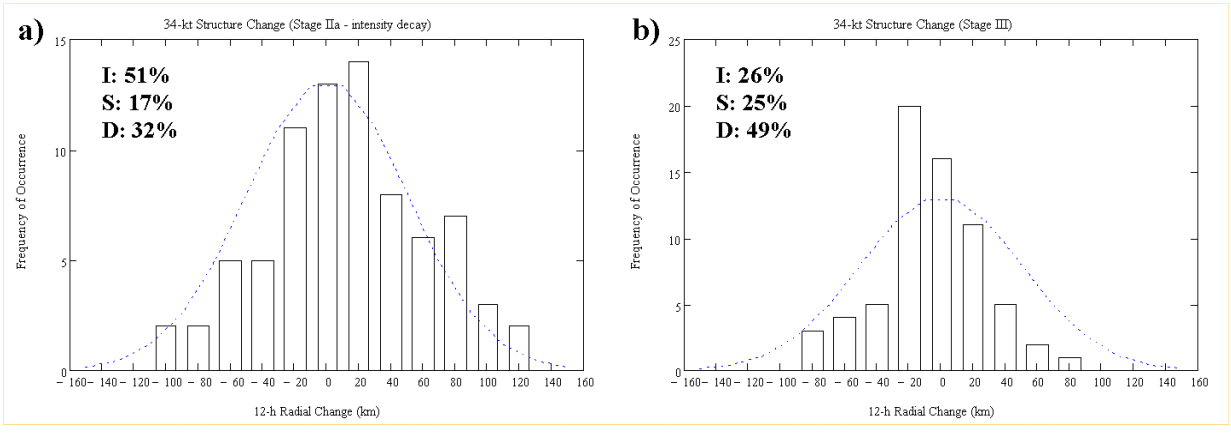

Fig. 8. Histograms of 12-h axisymmetric outer wind structure changes in terms of R_{34} values as in Fig. 6, except for (a) Stage IIa – decay and (b) Stage III – decay.

stages in Figs. 6-8. Steady states for R_{50} and R_{64} changes over 12 h have been defined as ±7 km and ±3 km, respectively. These definitions were based on examination of the histograms of all analyses compared to a Gaussian distribution. Structure changes reflected by these radii can also be quite large over a 12-h period. For example, the 12-h R_{50} changes can be as large as ±99 km.

In summary, a significant fraction of R_{34} changes over 12 h during the intensification or re-intensification phases are decreases rather than the increases that would be expected from the simple conceptual models discussed in section 5a. Similarly, a significant fraction of R_{34} increases over 12 h are found during the decay phases when decreases might have been expected from the simple conceptual model. However, Merrill (1984, 1988) had suggested that the radii of the closed isobars increase during the decay phase and Knaff et al. (2007) model has a latitudinal dependence that may predict R_{34} increases at latitudes greater the 25°N where decay is expected. Thus, these axisymmetric (and quadrant-by-quadrant, not shown) R_{34} changes are more complicated than the simple conceptual model that directly correlates R_{34} changes to intensity changes.

These life cycle histograms may indicate two possibilities: (i) structure change is random and unpredictable; or (ii) identifiable internal and external mechanisms exist that lead to the observed structure changes. Through analysis of individual storm cases as in Fig. 2, structure change mechanisms are being studied to prove the second possibility applies in the majority of the cases with large changes. Through examination of tropical cyclones that undergo similar structure changes, it may be possible to isolate the most probable mechanism(s) that lead to the changes observed. Individual storm analysis is currently in progress by examining cases of large R_{34} and R_{50} changes that may be explainable in terms of the internal or external mechanisms that have been proposed for structure changes.

6. TROPICAL CYCLONE WIND STRUCTURE

6.1 H*Wind Dataset Comparisons

Moyer et al. (2007) analyzed 691 H*Wind analyses generated for 69 Atlantic basin tropical cyclones during the 2000-2005 hurricane seasons. Through the use of multiple statistical analyses of the outer wind radii, they demonstrated that the H*Wind dataset presents a physically realistic representation of the outer wind radii. However, a comparison of the H*Wind dataset with the National Hurricane Center (NHC) Best Track re-analyses during the 2004 and 2005 hurricane seasons showed some inconsistence. In their comparison, statistically significant differences were noted with H*Wind R_{34} wind radii being found to be consistently larger than the NHC Best Track wind radii for all Saffir-Simpson categories of hurricanes (i.e., Category 1 through Category 5).

In the current study, an objective analysis was performed using a subgrid analysis technique on each of the 6 km^2 H*Wind gridded analyses provided by HRD (NOAA 2007) during the 2003-2005 Atlantic hurricane seasons to determine the average R_{34} wind radii in each Cartesian quadrant (i.e., NW, NE, SE, and SW). Prior to generating the resulting comparison in Fig. 9, all data (by quadrant) was screened and eliminated if the R_{34} wind radii intersected any land mass (except very small islands). The extended best track (EBT; Demuth 2006) dataset was used to compare the calculated R_{34} wind radii from the gridded H*Wind analyses. Comparison of the EBT wind radii to the H*Wind wind radii was facilitated by using a time-weighted linear interpolation of the EBT dataset to match the H*Wind analysis times.

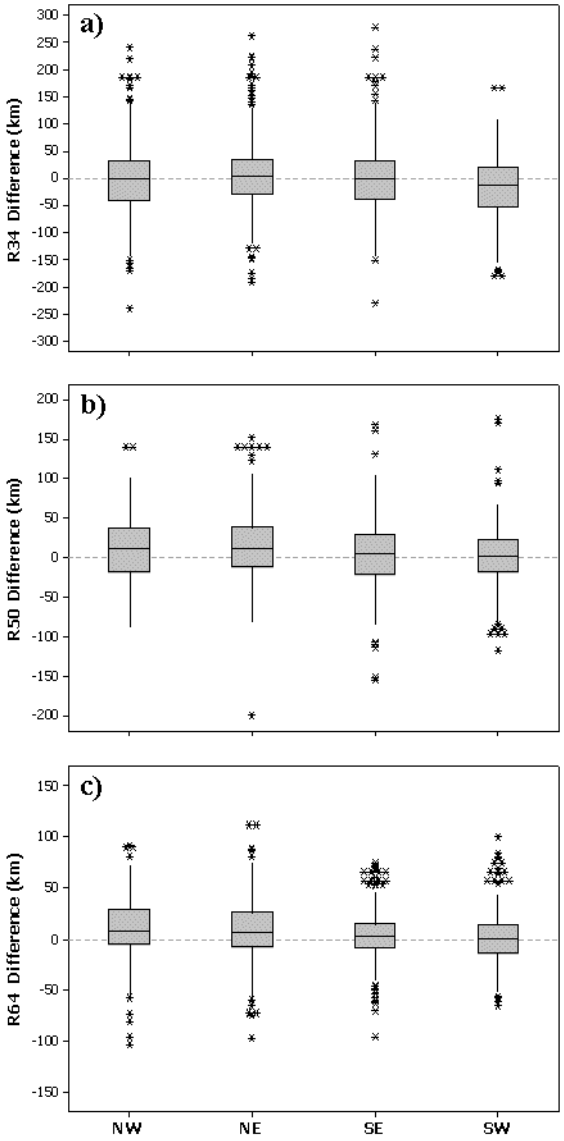

Fig. 9. Comparison of the EBT wind radii to H*Wind analyzed wind radii for the Atlantic tropical cyclone radii at (a) R_{34}, (b) R_{50}, and (c) R_{64} for each Cartesian quadrant: northwest (NW), northeast (NE), southeast (SE), and southwest (SW).

Similar to the results of Moyer et al. (2007, their Fig. 7), a significant amount of variability is seen in all of the quadrants in Fig. 9a. However, (in the grouping of all Saffir-Simpson categories) no significant R_{34} biases are noted between the datasets with the exception of a small positive H*Wind radii bias in the SW quadrant (i.e., the H*Wind R_{34} wind radii are larger than the EBT wind radii). The R_{50} (Fig. 9b) and R_{64} wind radii (Fig. 9c) both show a negative H*Wind radii bias in the NW, NE, and SE quadrants (i.e., the H*Wind R_{50} and R_{64} wind radii are smaller than the EBT wind radii). Individual case comparative analyses (not shown) produce varied results in which one storm may compare well while another storm has large variances. Review of time sequential plots of individual cases seems to indicate the likelihood that the subjective assessments by various forecasters may bleed into the defined wind radii of the EBT dataset.

6.2 Variability of Outer Wind Structure

The use of schematic plots to display the tropical cyclone wind radii can be quite instructional. In Fig. 10, the H*Wind R_{34} wind radii are plotted for each Saffir-Simpson storm category and for each Cartesian quadrant. The box plot widths are proportional to the sample size used to compute the statistics. All land interaction within the R_{34} wind radii have been identified and eliminated from the plots. In addition, all trivial "zeros" have been eliminated from the plots, i.e., cases with a maximum wind speed less than tropical storm strength (<34 kt).

A broad overview of Fig. 10 reveals a general asymmetry in the R_{34} structure for most of the Saffir-Simpson categories. With the exception of Category 5 (H5) hurricanes, the NE quadrant has the largest structure size, the NW and SE quadrants are nearly equal in size, and the SW quadrant has the smallest structure size. The asymmetric distribution of R_{34} wind radii is partially explained by the addition or subtraction of the tropical cyclone motion vector (i.e., in the Atlantic basin storm motion generally adds to the winds in the NE quadrant and subtracts from the winds in the SW quadrant).

Increasing structure size of R_{34} wind radii from tropical storms (TS) through Category 2 (H2) hurricanes is readily apparent in Fig. 10 for all storm quadrants. The structure size of the R_{34} wind radii levels off for development between Category 2 (H2) and Category 4 (H4) hurricanes, expect in the southern quadrants where some size decrease is noted from Category 3 H3) to Category 4 (H4) hurricanes. Category 5 (H5) hurricanes appear to decrease in size for all quadrants.

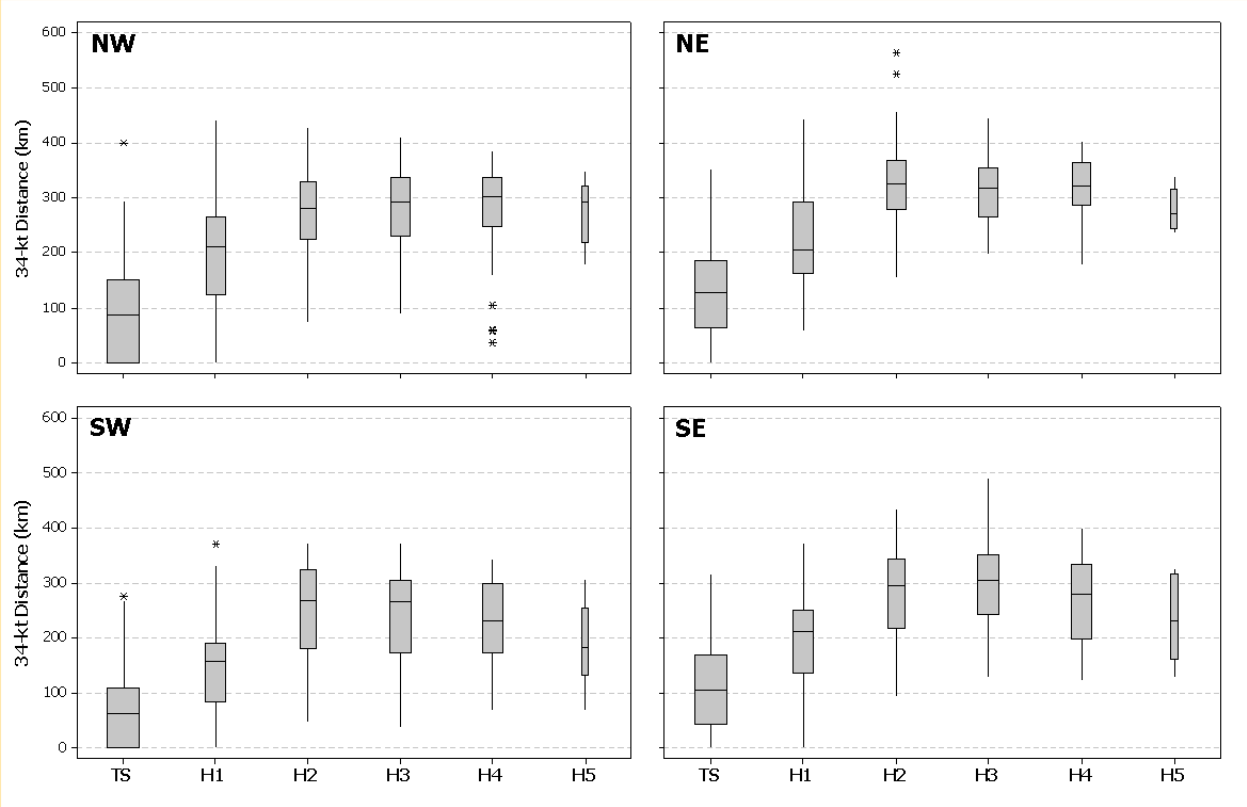

Fig. 10. Schematic plots of H*Wind R_{34} wind radii for Saffir-Simpson tropical storms (TS), Category 1 (H1) hurricanes, Category 2 (H2) hurricanes, Category 3 (H3) hurricanes, Category 4 (H4) hurricanes, and Category 5 (H5) hurricanes for each Cartesian quadrant: as in Fig. 9. The box plot widths are proportional to the sample size used to compute the statistics.

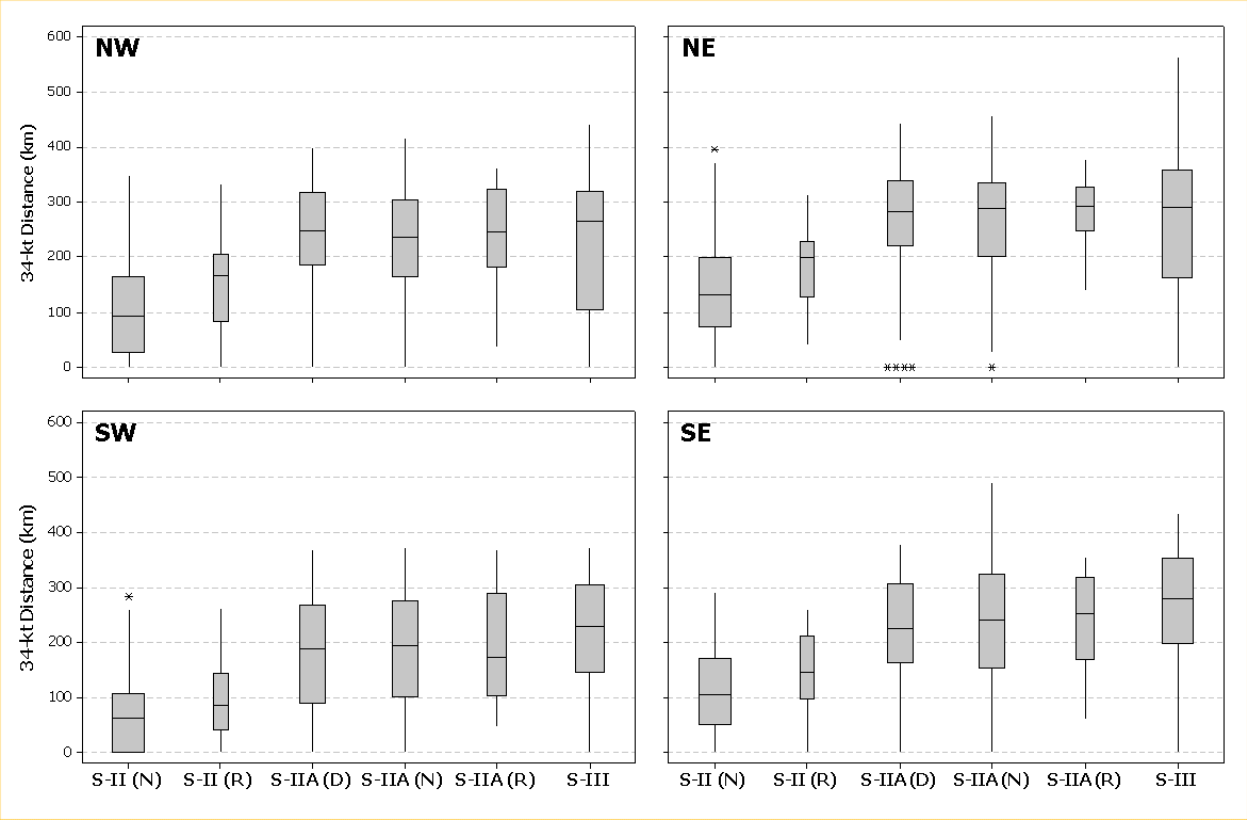

Fig. 11. Schematic plots of H*Wind R_{34} wind radii for Stage II (S-II) non-rapid (N) and rapid (R) intensification; Stage IIa (S-IIA) intensity decay (D), non-rapid (N) and rapid (R) intensification; and Stage III (S-III) for each Cartesian quadrant as in Fig. 9. The box plot widths are proportional to the sample size used to compute the statistics.

However, caution is advised in making any structure size interpretations of the Category 5 (H5) hurricane data for R_{34} wind radii, since the sample size (n=8) is too small to be considered statistically sound.

In Fig. 11, the H*Wind R_{34} wind radii are plotted for each stage of tropical cyclone development (as defined in section 5.2) for each Cartesian quadrant. The box plot widths are proportional to the sample size used to compute the statistics. All land interactions within the R_{34} wind radii have been identified and eliminated from the plots. In addition, all trivial "zeros" have been eliminated from the plots, i.e., cases with a maximum wind speed less than tropical storm strength (<34 kt). Tropical cyclone formation (i.e., Stage I) is not displayed since by definition these cases have no wind speeds above 34 kt. In addition and as noted earlier, the sample size for Stage I development is very limited.

A similar asymmetric R_{34} structure size is revealed in Fig. 11 as seen in Fig. 10. This asymmetric structure is apparent through each stage of tropical cyclone development for the same reasons as noted earlier. Sample sizes are large enough ($n \geq 30$) to ensure statistical sound results for all stages of development. Ideally, the sample size of Stage II (S-II) rapid (R) intensification should be larger. However, the sample sizes of S-II (R) in all four quadrants is very close to 30 cases and therefore deemed as representative of the larger statistical population.

Stage II (S-II) rapid (R) intensification consistently indicates a greater R_{34} structure size in all four quadrants (Fig. 11). From this result, one might hypothesize that the outer wind structure either plays a role in rapid intensification or is indicative of a favorable environment for rapid intensification. Further study is needed to address this finding and will be pursued as part of the current research effort.

The most rapid R_{34} structure size growth in Fig. 11 is noted during the Stage IIa (S-IIA) intensity decay (D) phase of tropical cyclone development. This data observation is consistent with the findings of Terwey and Montgomery (2008) in their idealized high-resolution numerical simulation of secondary eyewall replacement. The implications of the observational data and the numerical study suggest that outer wind radii increase the most during the S-II (D) phase of storm development. Once again, further study is needed and will be pursued as part of the current research effort.

Non-rapid (N) and rapid (R) intensification during Stage IIa (S-IIA) show little change in R_{34} structure size with the exception of a size decrease in the SW quadrant (Fig. 11). During Stage III (S-III), the R_{34} wind radii increase in all quadrants except the NE quadrant. This observation is inconsistent with the predicted size decrease by the modified Rankine vortex, but validates forecaster rules-of-thumb that call for an expansion of the tropical cyclone R_{34} wind radii during the decay phase of the tropical cyclone.

7. CONCLUSIONS

Advances are beginning to be made in the understanding of tropical cyclone outer wind structure changes, which are important both directly for forecasting the time when damaging winds will arrive and indirectly via their beta-effect propagation. A numerical modeling study by Terwey and Montgomery (2008) suggests surprisingly large increases in the radius of 50 kt (R_{50}) and 34 kt (R_{34}) winds may occur during secondary eyewall formations and is observed in the statistical representation of wind radii in Fig. 11.

The simple conceptual model that an increase (decrease) in outer wind structure will occur during the intensification (decay) phases of a tropical cyclone is tested with a unique set of H*Wind analyses for Atlantic hurricanes. For a very small set of H*Wind analyses during the formation phase, increases in R_{34} are noted. However, a considerable percentage of R_{34} decreases occur during the intensification phases when only increases would be expected. Likewise, a considerable percentage of R_{34} increases are observed in the decay phases when only decreases would be expected based on the simple conceptual model. The conclusion is that further study is required to understand the outer wind structure changes during the life cycle of the tropical cyclone.

Examination of the R_{34} structure size of tropical cyclones in the Atlantic and eastern North Pacific basins reveals fundamental flaws in simplified models, such as the modified Rankine vortex. While these vortex models are useful in many situations, they lack the complexity to account for atypical tropical cyclone structure changes during secondary eyewall replacement events and for special structure, such as annular hurricanes. Some intriguing questions about tropical cyclone structure and structure change remain to be answered. These are questions we hope to address in our ongoing research.

Acknowledgments: The participation by R. A. Stenger is supported by the Air Force Institute of Technology, and R. L. Elsberry is partially supported by the Office of Naval Research Marine Meteorology program. Dr. Mark Powell of HRD is acknowledged for his H*Wind analyses.

REFERENCES

Carr, L. E., III, and R. L. Elsberry, 1997: Models of tropical cyclone wind distribution and beta-effect propagation for application to tropical cyclone track forecasting. *Mon. Wea. Rev.*, **125**, 3190-3209.

Demuth, J., M. DeMaria, and J.A. Knaff, 2006: Improvement of advanced microwave sounder unit tropical cyclone intensity and size estimation algorithms. *J. Appl. Meteor.*, **45**, 1573-1581.

Elsberry, R. L., 2002: Predicting hurricane landfall precipitation: Optimistic and pessimistic views from the Symposium on Precipitation Extremes. *Bull. Amer. Meteor. Soc.*, **83**, 1333-1340.

_____, T. D. B. Lambert, and M. A. Boothe, 2007: Accuracy of Atlantic and eastern North Pacific tropical cyclone intensity forecast guidance. *Wea. Forecasting*, **22**, 747-762.

_____, and R. A. Stenger, 2008: Advances in understanding of tropical cyclone wind structure change. *Asian-Pacific J. Atmos. Sci.*, **44**, 11-24.

Emanuel, K.A., 1995a: The behavior of a simple hurricane model using a convective scheme based on subcloud-layer entropy equilibrium. *J. Atmos. Sci.*, **52**, 3959-3968.

_____, 1995b: Sensitivity of tropical cyclones to surface exchange coefficients and a revised steady-state model incorporating eye dynamics. *J. Atmos. Sci.*, **52**, 3969-3976.

Fiorino, M., and R. L. Elsberry, 1989: Some aspects of vortex structure related to tropical cyclone motion. *J. Atmos. Sci.*, **46**, 975-990.

Hawkins, J. D., M. Helveston, T. F. Lee, F. J. Turk, K. Richardson, C. Sampson, J. Kent, and R. Wade, 2006: Tropical cyclone multiple eyewall configurations. Paper 6B.1, *27th Hurr. And Trop. Meteor. Conf.*, Monterey, CA, Amer. Meteor. Soc., Boston, MA.

Kimball, S. K., and M. S. Mulekar, 2004: A 15-year climatology of North Atlantic tropical cyclones. Part 1: Size parameters. *J. Climate*, **17**, 3555-3575.

Knaff, J. A., J. P. Kossin, and M. DeMaria, 2003: Annular hurricanes. *Wea. Forecasting*, **18**, 204-223.

_____, T. A. Cram, A. B. Schumacher, J. P. Kossin, and M. DeMaria, 2008: Objective identification of annular hurricanes. *Wea. Forecasting*, **23**, 17-28.

Merrill, R. T., 1984: A comparison of large and small tropical cyclones. *Mon. Wea. Rev.*, **112**, 1408-1418.

_____, 1988: Environmental influences on hurricane intensification. *J. Atmos. Sci.*, **45**, 1678-1687.

Moyer, A. C., J. L. Evans, and M. Powell 2007: Comparison of observed gale radius statistics. *Meteorol. Atmos. Phys.*, **45**, 1678-1687.

NOAA, cited 2007: Background on the HRD surface wind analysis system. Atlantic Oceanographic and Meteorological Laboratory (AOML), National Oceanic and Atmospheric Administration (NOAA). [Available at http://www.aoml.noaa.gov/.]

Pielke, R. A., and C. W. Landsea, 1998: Normalized hurricane damages in the United States: 1925-1995. *Wea. Forecasting*, **13**, 621-631.

Powell, M. D., and T. A. Reinhold, 2007: Tropical cyclone destructive potential by integrated kinetic energy. *Bull. Amer. Meteor. Soc*., **88**, 513-526.

_____, S. H. Houston, and T. A. Reinhold, 1996: Hurricane Andrew's landfall in south Florida. Part I: Standardizing measurements for documentation of surface wind fields. *Wea. Forecasting*, **11**, 304-328.

_____, _____, L. R. Amat, and N. Morisseau-Leroy, 1998: The HRD real-time hurricane wind analysis system. *J. Wind. Eng. Ind. Aerodyn*., **77-78**, 53-64.

Terwey, W. D., and M. T. Montgomery, 2008: Secondary eyewall formation in two idealized, full-physics modeled hurricanes. *J. Geophys. Res., (Atmos.)*, in press.

Willoughby, H. E., J. A. Clos, and M. G. Shoreibah, 1982: Concentric eyewalls, secondary wind maxima, and the evolution of the hurricane vortex. *J. Atmos. Sci*., **39**, 395-411.